Reconfigurable Complementary Monolayer $MoTe_2$ Field-Effect Transistors for Integrated Circuits

Supporting Information

Stefano Larentis, Babak Fallahazad, Hema C. P. Movva, Kyounghwan Kim, Amritesh Rai, Takashi Taniguchi†, Kenji Watanabe†, Sanjay K. Banerjee and Emanuel Tutuc.

Microelectronics Research Center, Department of Electrical and Computer Engineering, The University of Texas at Austin, Austin, TX 78758, USA

†National Institute for Materials Science, 1-1- Namiki Tsukuba, Ibaraki 305-0044, Japan

Contents

S1: Optical micrographs of monolayer $MoTe_2$

Figure S1 shows a set of optical micrographs of a $MoTe_2$ flake taken at different times after the exfoliation, showing a decrease in optical contrast of the monolayer (ML) region with time. MLs are left in atmosphere after the exfoliation. Figure 2a-c, in the main text, shows a ML flake becoming effectively invisible under optical microscopy after 5 days, compared to the ML in Figure S1 which undergoes a similar contrast variation in 18 hours, showing how contrast evolves differently for each flake. For thicker $MoTe_2$ flakes, no apparent change in the contrast is noticeable.

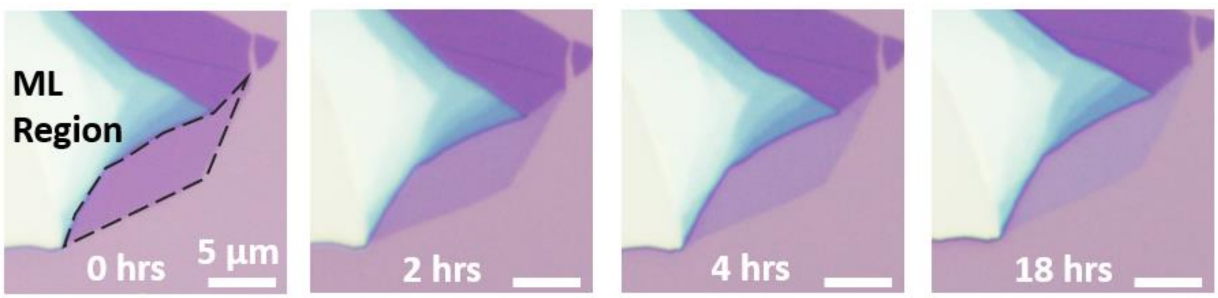

Figure S1. (a-c) Optical micrographs of a $MoTe_2$ flake exfoliated on SiO_2/Si wafer, with 285 nm SiO_2 thickness. The optical contrast decreases with time in the exposed monolayer region.

S2: Intensity ratio of ML $MoTe_2$ E^1_{2g} and Si 520 cm^{-1} peaks as a function of time

Figure 2d, in the main text, shows ML $MoTe_2$ Raman spectra for exposed and encapsulated regions, and its variation over time. Raman spectra are acquired with a Renishaw In-Via system, using a 532 nm excitation wavelength, a 100X objective lens (~1 μm spot size) and an excitation power, measured at the microscope objective, ranging between 20 and 100 μW. Figure S2 shows the intensity ratio of ML $MoTe_2$ E^1_{2g} and Si 520 cm^{-1} peaks ($I_{E^1_{2g}}/I_{Si}$) as function of time, summarizing a larger set of data acquired from 7 different $MoTe_2$ MLs, for both exposed and encapsulated flakes. In between Raman spectra measurements the flakes are left in atmosphere.

Figure S2a,d shows a set of $I_{E^1_{2g}}/I_{Si}$ data as a function of time, for exposed $MoTe_2$ MLs, using an excitation power of 100 μW and 20 μW, respectively. Each flake is characterized by a different $I_{E^1_{2g}}/I_{Si}$ decay rate. All flakes measured register a $I_{E^1_{2g}}/I_{Si}$ reduced in half after 24 hours, showing it is critical to encapsulate the flakes as soon as possible after the exfoliation.

Figure S2b,e shows $I_{E^1_{2g}}/I_{Si}$ data as a function of time, for partially encapsulated $MoTe_2$ MLs, using an excitation power setting of 100 and 20 μW, respectively. Red (black) data sets refer to areas where the $MoTe_2$ is encapsulated (exposed), as shown by the corresponding marker on the related optical micrograph (Figure S2c,f). $I_{E^1_{2g}}/I_{Si}$ data for the exposed region show a decreasing intensity ratio over time, while the encapsulated one show a constant intensity ratio, independent of the laser power. The ML $MoTe_2$ Raman spectra remains consistent for over 10 days in encapsulated samples.

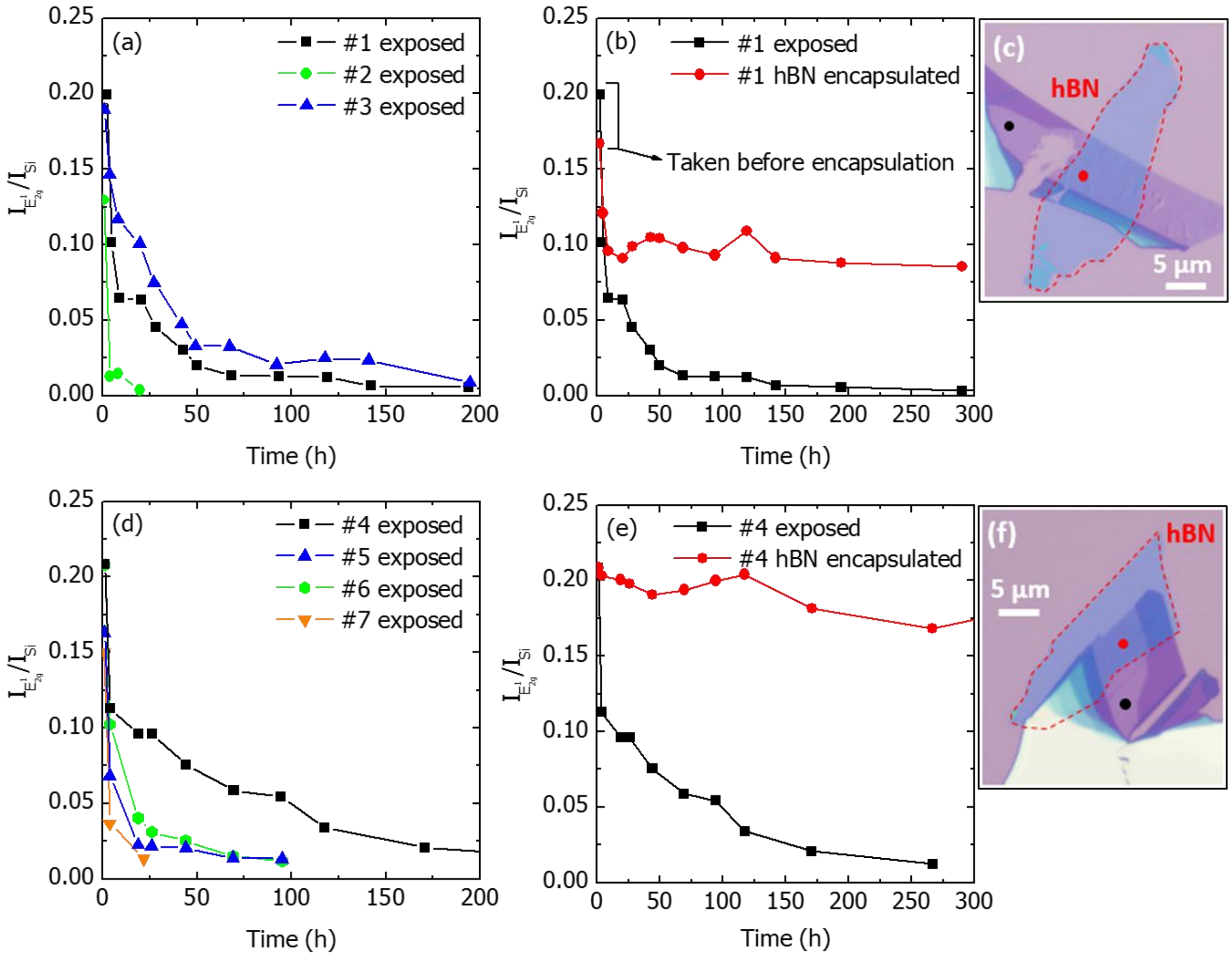

Figure S2. (a,d) $I_{E^1_{2g}}/I_{Si}$ measured as a function of time, for different $MoTe_2$ MLs, using an excitation power of 100 µW in (a), 20 µW in (d). Each flake is characterized by a different $I_{E^1_{2g}}/I_{Si}$ decay rate. (b,e) $I_{E^1_{2g}}/I_{Si}$ measured as a function of time, showing a decaying (constant) intensity ratio over time for the exposed (encapsulated) regions of the sample, measured using an excitation power of 100 µW in (b), 20 µW in (e). (c,f) optical micrographs of the partially encapsulated flakes, with red (black) markers highlighting the encapsulated (exposed) region, referring to Raman spectra presented in panel (b) and (e), respectively.

S3: Top gate transfer characteristic and device stability

While Raman data confirm that hBN encapsulation prevents ML $MoTe_2$ environmental degradation, electrical measurements can provide another test of the hBN encapsulation effectiveness over longer periods of time. Figure S3, shows the top gate transfer characteristic (I_D vs. V_{TG}) at different drain biases (V_D), measured in vacuum, for a device using Pt bottom contacts, measured 7, and 21 days after the initial encapsulation. In between the measurements, the sample is stored in a vacuum desiccator. The two measurements are consistent, confirming the electrical stability of hBN-encapsulated $MoTe_2$ FETs.

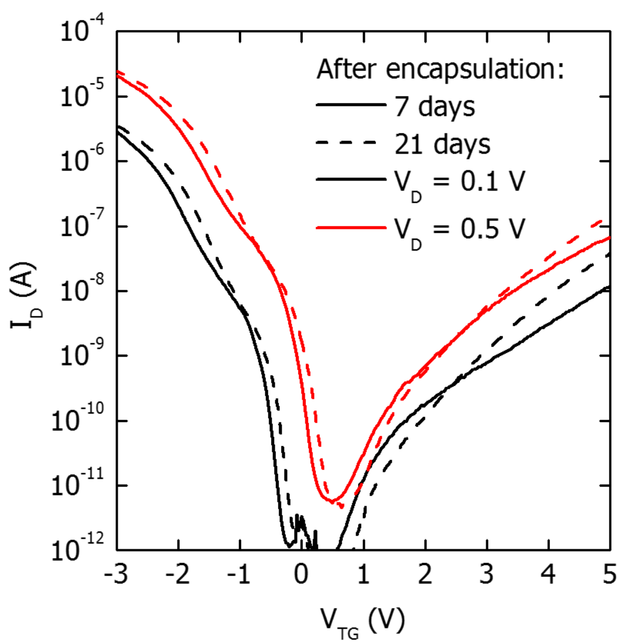

Figure S3. I_D vs. V_{TG}, measured at V_D = 0.1 and 0.5 V. The measurements are taken 7 days and 21 days after the device has been encapsulated in hBN (Width = 13 µm, Length = 1 µm, $t_{hBN\ top}$ = 8.2 nm).

S4: Mobility and contact resistance in bilayer $MoTe_2$

We describe the electrical characterization of a bottom contacted, top-gated, hBN encapsulated multi-terminal bilayer $MoTe_2$ device. Figure S4a shows an optical micrograph of the multi-terminal device structure. The top-gate metal overlaps both channel and bottom contacts, and modulates the carrier density in both regions. Figure S4b shows the top gate transfer characteristic (I_D vs. V_{TG}) measured at $V_D = \pm 0.1$ V, showing ambipolar characteristic; the back-gate is grounded in all measurements. Fig. S4c shows the measured 4-point conductance: $G_{4pt} = I_{DS}/(V_1\text{-}V_2)$ as function of V_{TG}, using the biasing scheme shown in Fig. S4a. We extract the μ_{FE} from the linear region of G_{4pt} transfer characteristic as follows:

$$\mu_{FE} = \frac{dG_{4pt}}{dV_{TG}} \frac{1}{C_{TG}\, W/L}$$

where $C_{TG} = 160$ nF/cm^2 is the capacitance of the 16.5 nm top hBN dielectric, estimated assuming a hBN relative dielectric constant of 3; W is the device width and L is the distance between two adjacent voltage probes (V_1 and V_2), marked in Fig. S4a. The extracted mobility values for each branch are $\mu_{FE,p} = 18$ cm^2/V·s and $\mu_{FE,n} = 8$ cm^2/V·s. The extracted $\mu_{FE,p}$ is comparable with previous $MoTe_2$ results in literature, see Ref. 14 in the main text. Once we determine R_{4pt}, the specific contact resistance R_C can be extracted as follows:

$$R_C = \frac{\mathrm{W}'}{2}\left(R_{2pt} - R_{4pt}\frac{L'}{L}\right)$$

where L' is the total device length, and W' is the source and drain contact width (marked in Fig. S4a), and $R_{2pt} = V_{DS}/I_{DS}$ is the 2-point resistance. Fig. S4d shows R_C as a function of V_{TG}, with R_C decreasing for increasing $|V_{TG}|$. This reflects the top-gate tuning the carrier density in proximity of bottom contacts, electrostatically doping the contact regions, thus modulating R_C. The R_C values extracted using this multi-terminal structure are comparable with the tunable R_C obtained by setting fixed contact gate biases (V_{CG}s) in the 2-point devices presented in the main text.

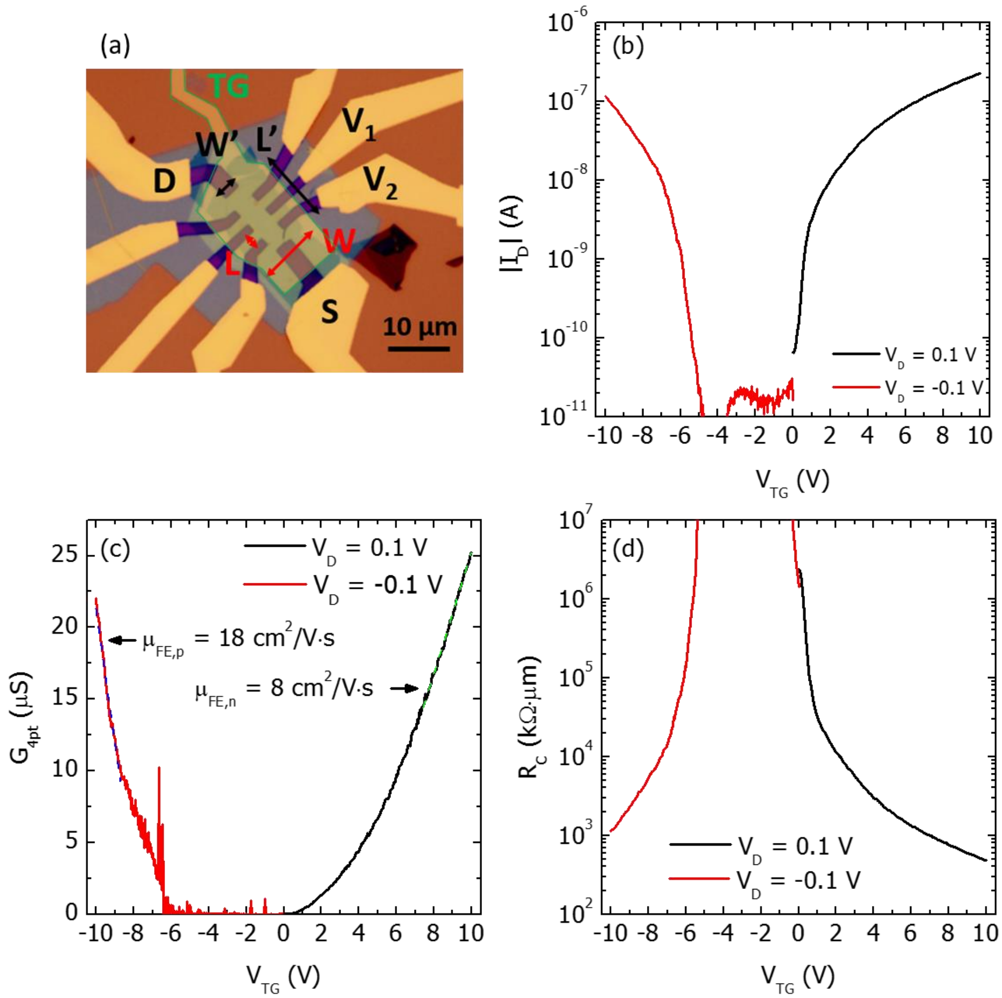

Figure S4. (a) Optical micrograph of the device. (a) $|I_{DS}|$ vs. V_{TG} measured at $V_D = \pm 0.1$ V for a top-gated bilayer $MoTe_2$ device with Pt contacts ($W = 10$ µm, $L = 3.1$ µm, $L' = 11.4$ µm, and $W' = 3.2$ µm). (b) G_{4pt} vs. V_{TG} measured at $V_D = \pm 0.1$ V, dashed lines represent a linear fit used to extract the μ_{FE}. (c) R_C vs. V_{TG} measured at $V_D = \pm 0.1$ V, showing a decreasing R_C with increasing $|V_{TG}|$, reflecting the top-gate modulation of the contact regions.